

Polariton Condensation in photonic molecules

Marta Galbiati,¹ Lydie Ferrier,¹ Dmitry D. Solnyshkov,² Dimitrii Tanese,¹ Esther Wertz,¹ Alberto Amo,¹ Pascale Senellart,¹ Isabelle Sagnes,¹ Aristide Lemaître,¹ Elisabeth Galopin,¹ Guillaume Malpuech,² and Jacqueline Bloch¹

¹*CNRS-Laboratoire de Photonique et Nanostructures, Route de Nozay, 91460 Marcoussis, France*

²*LASMEA, CNRS, Clermont University, University Blaise Pascal,*

24 avenue des Landais, 63177 Aubière cedex, France

(Dated: October 4, 2011)

We report on polariton condensation in photonic molecules formed by two coupled micropillars. We show that the condensation process is strongly affected by the interaction with the cloud of uncondensed excitons. Depending on the spatial position of these excitons within the molecule, condensation can be triggered on both binding and anti-binding polariton states of the molecule, on a metastable state or a total transfer of the condensate into one of the micropillars can be obtained. Our results highlight the crucial role played by relaxation kinetics in the condensation process.

PACS numbers: 71.36.+c, 67.85.Hj, 78.67.Pt, 78.55.Cr

Most of the experimental studies in atomic Bose condensates have explored conditions of thermodynamic equilibrium since typical condensate lifetimes are much longer than interaction times. Recent theoretical proposals have shown that out of equilibrium bosonic systems present qualitatively new behaviors [1]. One proposed way to reach this regime is the use of photonic systems with effective photon-photon interactions and dissipation provided by inherent optical losses [2]. Localized to delocalized phase transitions [3, 4], highly entangled states [5], or fermionisation effects in a ring of coupled sites [6] are predicted in such systems.

Microcavity polaritons are a model system for the investigation of the physics of driven-dissipative boson condensates [7–13]. They are the quasi-particles arising from the strong coupling between excitons confined in quantum wells and the optical mode of a microcavity. Because of their light-matter nature, polaritons present peculiar properties: they interact efficiently with their environment through their excitonic part [14, 15] while their photonic part enables efficient coupling with the free space optical modes. Polariton condensates can be generated in zero dimensional micropillars [11] or in arrays of pillars with fully controlled coupling [16, 17]. In this configuration, the non-equilibrium nature of polariton condensates should allow the realization of metastable collective states, such as the self-trapped states in a bosonic Josephson junction [18–20].

In the present paper we investigate polariton condensation in photonic molecules obtained by coupling two micropillars. We demonstrate that polariton interactions strongly affect the way condensation occurs in such coupled system, not only modifying the wavefunction of the polariton condensate, but also the relaxation dynamics. This effect, specific to an out-of-equilibrium bosonic system, is illustrated by considering different positions of the non resonant excitation within the molecule. When the excitation spot is placed at the center of the molecule, polariton condensation is observed on both binding and

anti-binding states. Interactions induce strong changes in the condensate wavefunction, the most important one being the change in its spatial anisotropy.

When the excitation spot is positioned on one of the two coupled micropillars, condensation occurs in a very different way. As the excitation power is increased, the polariton condensate is first created in a metastable state localized in the excited pillar by an effect similar to self trapping[18]. Further increasing the pumping power, the condensation tends to progressively evolve from a kinetic regime to a regime closer to thermodynamical equilibrium: massive occupation is observed on the lowest energy state of the system, mainly localized in the non-excited pillar. These results are simulated using a relaxation model including semi-classical Boltzmann equations and nonlinear Schrödinger equation in a self-consistent way. The key features of our experiments can only be reproduced if one properly includes the changes of the relaxation rates due to interaction-induced modifications of the overlaps between the different polariton states.

The microcavity sample, described in Ref. [11], consists in a $\lambda/2$ cavity with a quality factor exceeding 16 000 and containing 12 GaAs quantum wells. Coupled micropillars were fabricated using electron beam lithography and Inductively Coupled Plasma dry etching. The diameter d of the micropillars ranges from 3 to 4 μm and their center to center distance d_{CC} is varied from 2.3 to 3.7 μm , corresponding to an expected coupling constant between 0.1 and 1 meV . Note that d_{CC} is always kept smaller than twice the radius of the pillars, ensuring the direct coupling of the polariton modes of the two micropillars. A scanning electron micrograph of an array of such photonic molecules is shown in Fig.1.a. Microphotoluminescence experiments are performed on single molecules using a single mode cw Ti:Saph laser focused onto a 2 μm diameter spot with a microscope objective. The sample is maintained at 10 K and the excitation laser energy is tuned typically 100 meV above the lower polariton reso-

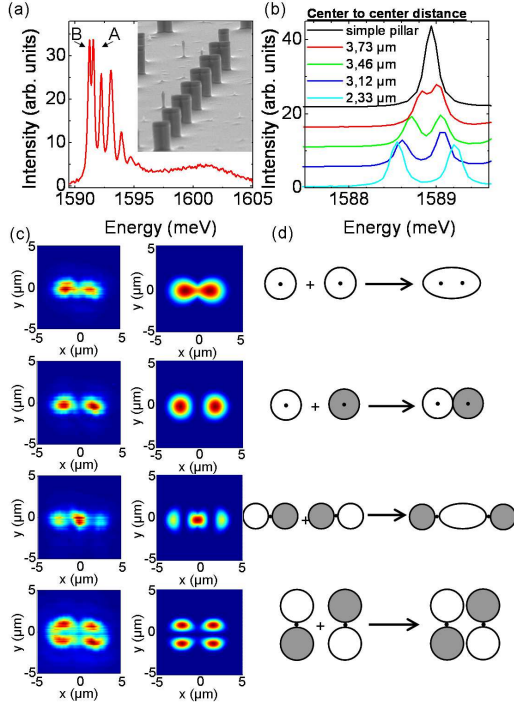


FIG. 1: (Color online) (a) Emission spectrum measured on a single molecule at low excitation power ($d = 4 \mu\text{m}$ and $d_{CC} = 3.73 \mu\text{m}$); A and B indicate the binding and anti-binding states. Inset : scanning electron micrograph of an array of pillars and molecules. b) Emission spectra measured on a $4 \mu\text{m}$ round micropillar (black line) and on photonic molecules with $d = 4 \mu\text{m}$ and various values of d_{CC} . c) left (resp. right) column : measured (resp. calculated) emission pattern of the four lowest energy modes of a photonic molecule with $d = 4 \mu\text{m}$ and $d_{CC} = 3.73 \mu\text{m}$; d) Schematic of the hybridization of the individual pillar modes within a photonic molecule.

nance, thus providing non-resonant optical excitation of the system. The emission is collected through the same objective and imaged on the entrance slit of a monochromator. The spectrally dispersed emission is detected with a nitrogen-cooled CCD camera. We define the detuning $\delta = E_c - E_x$ as the energy difference between the lowest energy photonic mode and the exciton resonance.

The polariton modes in these photonic molecules are investigated by photoluminescence measurements at low excitation power. An example of an emission spectrum measured on a single molecule is presented in Fig. 1.a. Discrete emission peaks are observed corresponding to polariton quantum states fully confined in the microstructure. The broader line at higher energy is due to emission of the excitonic reservoir. The two lowest energy modes (labeled B and A) are attributed to the binding and anti-binding states arising from the hybridization of the lowest energy mode of each micropillar. The splitting between these states is proportional to the coupling between the two micropillars. It can be contin-

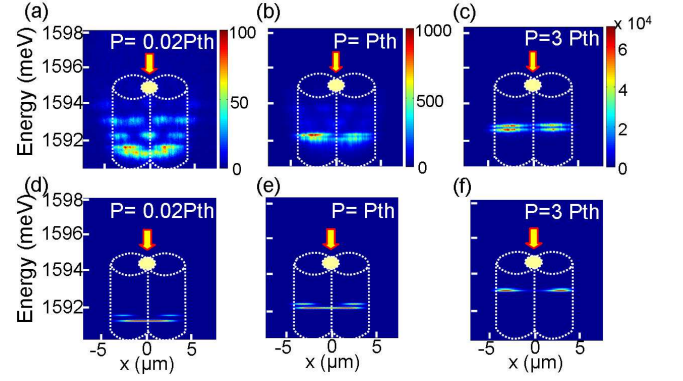


FIG. 2: (Color online) **Excitation at the center of the molecule:** a)-c) Spectrally resolved emission distribution along the molecule axis measured for several excitation powers; d)-f) Calculated emission patterns for several excitation powers. $d = 4 \mu\text{m}$ and $d_{CC} = 3.46 \mu\text{m}$. $\delta = -3 \text{ meV}$

uously tuned by changing the center to center distance d_{CC} , as illustrated in Fig. 1.b. The left column of Fig. 1.c shows the spatial distribution (near field) of the four lowest energy modes in a molecule made of two $4 \mu\text{m}$ pillars with $d_{CC} = 3.73 \mu\text{m}$ (the first two panels correspond to the B and A modes). The right column shows the calculated polariton wavefunctions considering a confinement potential taken as infinite outside the photonic molecule and equal to zero inside. As schematically illustrated in Fig. 1.d, all these states result from the hybridization of the optical modes of each individual micropillar, showing the strong analogy between our system and the orbitals of a diatomic molecule.

We now discuss polariton condensation in these molecules under non resonant optical excitation. As we have shown in our recent work on single micropillars [21], such an excitation scheme not only populates the confined polariton states, but also creates a population of uncondensed excitons called the excitonic reservoir. Because of the limited diffusion length of excitons, this reservoir remains localized in the excitation area. Repulsive interactions between polaritons and the excitonic reservoir strongly influence the precise quantum state in which polaritons accumulate. In the following we will consider two different locations of the excitonic reservoir within the molecule, which can be selected via the position of the excitation laser spot. First we will consider excitation conditions where the reservoir of uncondensed excitons is at the center of the molecule. Then we will address the case of asymmetric excitation, in which the excitonic reservoir is injected only in one of the two micropillars. Specific spatial behavior of the polariton condensates is observed in each case, driven by the polariton interaction with the excitonic reservoir.

Figure 2.a-c present the measured emission distribution along the axis of a photonic molecule excited at its

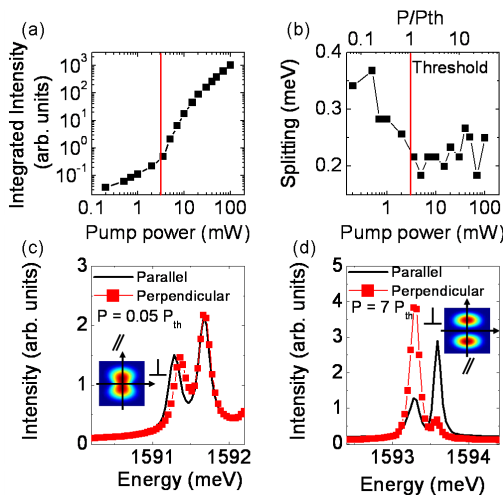


FIG. 3: (Color online) **Excitation at the center of the molecule:** a) Integrated intensity measured as a function of the excitation power; b) Splitting between the two lowest energy emission lines measured as a function of the excitation power; c) Lowest energy emission lines measured with a polarization parallel (solid line) and perpendicular (squares) to the molecule axis for $P = 0.05 P_{th}$; d) same as c) for $P = 7 P_{th}$. The inset shows the calculated spatial shape of the binding state

center. As summarized in Fig. 3.a, above a well defined excitation threshold, a strong non-linear increase of the emission intensity is observed, one of the signatures of polariton condensation [11]. Under this excitation condition, a massive accumulation of polaritons occurs both in the binding and anti-binding lowest energy polariton states. Interestingly, as the excitation power is increased, a progressive change of the spatial shape of the polariton wavefunction is observed, with vanishing probability density at the center of the molecule. This behavior is due to repulsive interactions with the excitonic reservoir injected in that region.

To describe our experiments, we simulate polariton relaxation using coupled semi-classical Boltzman equations and nonlinear Schrödinger equations in a self-consistent way [22]. As described in the supplementary information, on one hand, a nonlinear Schrödinger equation is solved at each time iteration, in the presence of the potential induced by the excitonic reservoir and by the occupation of the polariton states, to find the eigenstates of the system. On the other hand, the time evolution of these occupation numbers are calculated using the semi-classical Boltzmann equations in which the scattering rates are obtained using the exact shape of the polariton states obtained from the non-linear Schrödinger equation. Both exciton-phonon and exciton-exciton scattering mechanisms are considered. The reservoir is assumed to be thermalized at the lattice temperature. The key ingredient to describe our experiments is to consider scat-

tering rates proportional to the spatial overlap between initial and final states. For instance, the scattering rate of two excitons from the reservoir resulting in one polariton in state i and one exciton in the reservoir is proportional to $\int |\psi_i(x, y)|^2 (\rho_R(x, y))^3 dx dy$, where $\psi_i(x, y)$ is the wavefunction of the polariton state i and $\rho_R(x, y)$ is the spatial distribution of the excitonic reservoir, described by a gaussian of width w_R . To fit the data we use an exciton-exciton scattering rate $W_{XX} = 2 \cdot 10^3 \text{ s}^{-1}$ and an exciton-phonon scattering rate $W_{XP} = 10^9 \text{ s}^{-1}$. The lifetime of the reservoir is equal to 400 ps , and that of the polariton states to 30 ps , a value extracted from coherence measurements in ref.[12].

The results of the model for central pumping are shown in Fig. 2d-f. The potential of the reservoir increases with the optical pumping and has a maximum at the center of the molecule, inducing the spatial separation of the states of each micropillar. As a result, both the coupling and the associated splitting between the two lowest energy states decrease. Indeed, this feature is shown in Fig. 3.b: simultaneous to the spatial separation of the polariton distributions, the measured splitting goes down to a minimum at about $P = 4 P_{th}$. At higher powers, the measured splitting tends to increase again. In the following, we will show that at such high density the observed splitting is no longer related to the binding anti-binding splitting but is an anisotropic splitting induced by the lateral spatial shrinking of the condensate wavefunction in each micropillar. This feature is not reproduced by our model which does not include the polarization degree of freedom.

Polarization resolved measurements were performed for different excitation densities. Figure 3.c and 3.d display emission spectra linearly polarized parallel and perpendicular to the molecule axis, below and above threshold. In the low density regime (Fig. 3.c), the presence of uncondensed excitons has a negligible effect, and we observe a polarization splitting in both the binding and anti-binding states. As previously reported theoretically and experimentally [23], this splitting is larger for the binding state and amounts to $70 \mu\text{eV}$. The inset of Fig.3.c shows that the overall shape of the polariton binding state is elongated along the molecule. This is why the lowest energy line of the binding state doublet is polarized parallel to the molecule axis. The situation is different at high density ($P > 4 P_{th}$), where a stronger potential barrier is induced by the excitonic reservoir at the center of the molecule. In this case, the coupling between the states of each micropillar becomes too small to be resolved in our experiment. The remaining splitting is then purely a polarization splitting. In each micropillar, the polariton wavefunction is shrunk by the excitonic repulsive potential and thus it is more elongated perpendicularly to the molecule axis. This change in anisotropy is evidenced in the polarization of the emission. The lowest energy emission line is now strongly polarized perpendic-

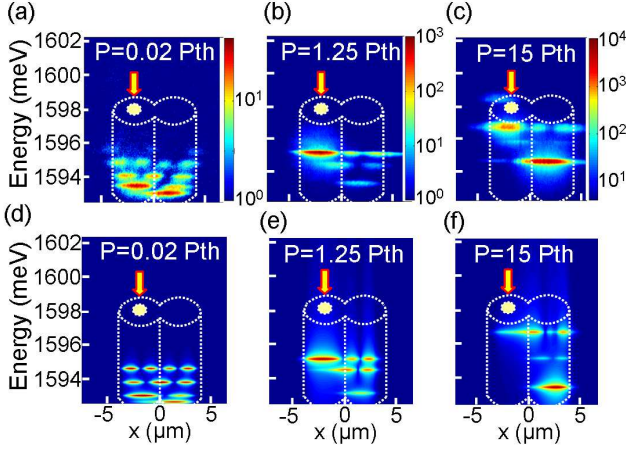


FIG. 4: (Color online) **Asymmetric Excitation:** a)-c) Spectrally resolved emission distribution along the molecule axis measured for several excitation powers; d)-f) Calculated emission patterns for several excitation powers. $d = 3.5 \mu\text{m}$ and $d_{CC} = 3.1 \mu\text{m}$. $\delta = -3 \text{ meV}$

ular to the molecule axis.

Different dynamics is observed when the laser spot is positioned on top of one of the micropillars forming the molecule. Emission distributions measured under these conditions are reported in Fig. 4.a-c. Close to threshold, condensation occurs in the pillar that is optically pumped. Interparticle interactions blue shift the energy of the ground state in the pumped pillar, decoupling it from the states of the other pillar, and severely limiting the Josephson transfer of particles from one pillar to the other. This localisation is very analogous to the original self-trapping effect, except that here the blue shift is mainly induced by the interaction between the exciton reservoir and the condensate and not by interactions within the condensate itself. As the excitation power is increased, the better relaxation kinetic and the presence of excited states in the un-pumped pillar destroy the metastable state [24] and allow the system reaching its ground state. Condensation then occurs in the non-pumped micropillar (Fig. 4.c).

We can reproduce this overall behavior using the self-consistent polariton relaxation model presented above. As shown in Fig. 4.d, at low power the reservoir potential creates an asymmetry in the two bottom states of the molecule, whereas the upper states are not affected. The populations of the excitonic states in the reservoir are small and their relative distribution is given by the lattice temperature. When pumping increases (Fig. 4.e), condensation starts at the eigenstate possessing the largest overlap integral with the reservoir. This corresponds to the third polariton state (population n_3). The reservoir potential also significantly perturbs the two bottom states, which become both confined in the right pillar. This blocks the direct relaxation from the reservoir to-

wards these states and further enforce condensation in the third metastable state localized in the pumped pillar. At high pumping (Fig. 4.f) a new effect is observed: condensation is triggered onto the ground state (of population n_1). This does not arise from direct scattering from the reservoir, since the overlap between the ground state and the reservoir remains very small. This condensation is the result of efficient scattering from the intermediate third state toward the ground state via acoustic phonons. This regime occurs when the phonon assisted scattering rate $W_{XP}n_3(1+n_1)$ from the intermediate state into the ground state overcomes the ground state radiative losses $n_1\tau_1$. This happens when $n_3 \approx 100$ and further increase of the pumping does not change n_3 , but only increases n_1 . The second quantized state remains weakly populated: it has a smaller overlap with the reservoir than the third state and a higher energy than the ground state. Overall the complete condensation dynamics can only be understood considering the modifications of the relaxation rates induced by interactions (as shown in the supplementary [22] when constant scattering rates are considered, condensation in the metastable states can not be reproduced).

To conclude, we have demonstrated polariton condensation in photonic molecules, a fully controlled system in which the coupling constant between two condensates can be adjusted. Depending on the precise location of the excitonic reservoir, strong renormalization of the polariton states is induced, resulting in strong modification of the condensation dynamics. In particular condensation can occur in a metastable localized state, or in the ground state of the system. These results open the way towards a detailed investigation of Josephson oscillations [25] or, more generally, the pumped-dissipative physics of arrays of coupled condensates in an engineered environment.

This work was supported by the C’Nano Ile de France (Sophiie2), by the ANR (PNANO- 07-005 GEMINI), by the "Triangle de la Physique" (Picorre), by the FP7 ITN "Clermont4" (235114) and by the FP7 ITN "Spin-Optronics" (237252).

-
- [1] P. Werner et al., Phys. Rev. Lett. **94**, 047201 (2005).
 - [2] D. Gerace et al., Nature Physics **5**, 281 (2009)
 - [3] A. D. Greentree et al., Nature Phys. **2**, 856 (2006).
 - [4] S. Schmidt et al., Phys. Rev. B **82**, 100507(R) (2010).
 - [5] M. J. Hartmann et al., Nature Phys. **2**, 849 (2006).
 - [6] I. Carusotto et al., Phys. Rev. Lett. **103**, 033601 (2009).
 - [7] J. Kasprzak et al., Nature **443**, 409 (2006).
 - [8] R. Balili et al., Science **316**, 1007 (2007).
 - [9] C.W. Lai et al., Nature **450**, 529-532 (2007).
 - [10] S. Christopoulos et al., Phys. Rev. Lett. **98**, 126405 (2007).
 - [11] D. Bajoni et al., Phys. Rev. Lett. **100**, 047401 (2008).
 - [12] E. Wertz et al., Nature Phys. **6**, 860 (2010).

- [13] E. A. Cerda-Méndez et al., Phys. Rev. Lett. **105**, 116402 (2010)
- [14] F. Tassone and Y. Yamamoto Phys. Rev. B **59**, 10830 (1999)
- [15] C. Ciuti et al., Phys. Rev. B **62**, R4825 (2000)
- [16] M. Bayer et al., Phys. Rev. Lett. **81**, 2582 (1998)
- [17] G. Guttroff et al., Phys. Rev. E **63**, 036611 (2001).
- [18] A. Smerzi et al., Phys. Rev. Lett. **79**, 4950 (1997).
- [19] D. Sarchi et al., Phys. Rev. B **77**, 125324 (2008)
- [20] I. A. Shelykh et al., Phys. Rev. B **78**, 041302 (2008)
- [21] L. Ferrier et al., Phys. Rev. Lett. **106**, 126401 (2011).
- [22] Description of the model used to calculate polariton relaxation is found in the supplementary information.
- [23] S. Michaelis de Vasconcellos et al., Appl. Phys. Lett. **99**, 101103 (2011)
- [24] M.T. Trujillo-Martinez et al., Phys. Rev. Lett. **103**, 105302 (2009).
- [25] K. G. Lagoudakis et al., Phys. Rev. Lett. **105**, 120403 (2010).

Supplementary Information on "Polariton Condensation in photonic molecules"

Marta Galbiati,¹ Lydie Ferrier,¹ Dmitry D. Solnyshkov,² Dimitrii Tanese,¹
 Esther Wertz,¹ Alberto Amo,¹ Pascale Senellart,¹ Isabelle Sagnes,¹ Aristide
 Lemaître,¹ Elisabeth Galopin,¹ Guillaume Malpuech,² and Jacqueline Bloch¹

¹*CNRS-Laboratoire de Photonique et Nanostructures,*

Route de Nozay, 91460 Marcoussis, France

²*LASMEA, CNRS, Clermont University, University Blaise Pascal,*

24 avenue des Landais, 63177 Aubière cedex, France

(Dated: October 4, 2011)

Abstract

We describe in this supplementary information the model we have developed to simulate polariton relaxation in photonic molecules under the excitation conditions described in the paper. The results of these calculations are shown on figure 2 and 4 of the paper. Finally we show that the overall condensation dynamics is not reproduced if one does not take into account the interaction induced changes in the relaxation rates.

PACS numbers:

We simulate polariton relaxation in a self-consistent way, using coupled semi-classical Boltzmann equations and nonlinear Schrödinger equations. At $t = 0$ the system is empty and the pumping is switched on. We calculate the time evolution of the system until the establishment of a steady state. The nonlinear Schrödinger equation written below is used to find the spatial shapes and energies E_{i,t_j} of the polariton wave functions $\psi_{i,t_j}(x, y)$.

$$E_{i,t_j}\psi_{i,t_j} = -\frac{\hbar^2}{2m}\Delta\psi_{i,t_j} + \alpha\rho_R(x, y)N_R(t_j) + \alpha\left|\sum_i\psi_{i,t_{j-1}}e^{-iE_{i,t_{j-1}}t_j/\hbar}\right|^2\psi_{i,t_j} \quad (1)$$

m is the polariton effective mass. This equation is solved at time step t_j to find the eigenstates in presence of the potential created by the exciton reservoir (written as $\alpha\rho_R(x, y)N_R(t_j)$) and by the occupation of each polariton quantized states (last term of the equation). $\alpha = 6xE_b(a_B)^2$ is the exciton-exciton interaction constant, where x the exciton fraction of the considered quantum state (1 in the reservoir, 0.5 in the polariton states), E_b the exciton binding energy, a_B the exciton Bohr radius. $\rho_R(x, y)$ is the normalized reservoir density ($\int \rho_R(x, y) dx dy = 1$), $N_R(t_j)$ the number of excitons in the reservoir.

The reservoir is assumed to be thermalized at the lattice temperature: $n_R(E, t_j) = n_R(0, t_j) \exp(-E/k_B T)$. The total number of particles in the reservoir is $N_R(t_j) = 2 \sum_E n_R(E, t_j)$, where 2 stands for the spin degeneracy of bright heavy-hole excitons. Since excitons in the reservoir are confined in a quantum well, $N_R(t_j) = n_R(0, t_j) S m k_B T / 2\pi \hbar^2$, where S is the surface covered by the reservoir. $\rho_R(x, y)$ is assumed to be a Gaussian function with a width w_R close to the one of the excitation laser spot.

The time evolution of n_i , the occupation numbers of the quantized polariton states and of N_R , the reservoir population are calculated using semi-classical Boltzmann equations, taking into account both exciton-exciton and exciton-phonon interactions, as well as the presence of the thermalized excitonic reservoir.

For the quantized polariton states i the equation reads:

$$\begin{aligned}
\frac{dn_i}{dt} = & -\frac{n_i}{\tau_i} - n_i \sum_k (W_{XX} I_{ikRR} N_R + W_{XP}^{ik}) (n_k + 1) \begin{pmatrix} 1, k < i \\ e^{-E_{ik}/k_B T}, k > i \end{pmatrix} \\
& + (n_i + 1) \sum_k (W_{XX} I_{ikRR} N_R + W_{XP}^{ik} I_{ik}) n_k \begin{pmatrix} e^{-E_{ik}/k_B T}, k < i \\ 1, k > i \end{pmatrix} \\
& + (W_{XX} I_{iRRR} N_R + W_{XP}^{iR} I_{iR}) (N_R (n_i + 1) - n_i \frac{S m k_B T}{2\pi \hbar^2} e^{-E_{iR}/k_B T})
\end{aligned}$$

and for the reservoir state R the equation is:

$$\frac{dN_R}{dt} = P - \frac{N_R}{\tau_R} - \sum_i (W_{XX} I_{iRRR} N_R + W_{XP}^{iR} I_{iR}) \left(N_R (n_i + 1) - \frac{n_i S m k_B T}{2\pi \hbar^2} e^{-E_{iR}/k_B T} \right) \quad (2)$$

P is the non-resonant pumping populating the reservoir, $\tau_R = 400 \text{ ps}$ (resp. $\tau_i = 30 \text{ ps}$) is the excitonic reservoir (resp. polariton) lifetime. W_{XX} describes the exciton-exciton interaction rates. The exciton-phonon scattering rate reads:

$$W_{XP}^{ik,R} = W_{XP} e^{-\frac{(E_i - E_{k,R})}{\hbar c \frac{\pi}{a_B}}}$$

The wave vector conservation rule is replaced by an overlap integral between the spatial extensions of the initial and final states. The overlap integrals change with time, together with the shapes and the energies of the states according to equation (1). The overlap integrals involved are defined as follows:

$$\begin{aligned}
I_{ikRR} &= S^3 \int |\psi_i^* \psi_k|^2 \rho_R^2 \, dxdy, \\
I_{iRRR} &= S^3 \int |\psi_i|^2 \rho_R^3 \, dxdy
\end{aligned} \quad (3)$$

The overlap integrals obtained by summation of scattering rates with different phonon wavevectors read:

$$\begin{aligned}
I_{ik} &= S \int |\psi_i^* \psi_k|^2 \, dxdy, \\
I_{iR} &= S \int |\psi_i|^2 \rho_R \, dxdy
\end{aligned} \quad (4)$$

These overlap integrals are dimensionless.

Finally, the scattering rates W_{XX} and W_{XP} describing exciton-exciton and exciton-phonon interaction were used as the fitting parameters of the model, together with the width of the gaussian spatial distribution of the reservoir which we authorize to slightly

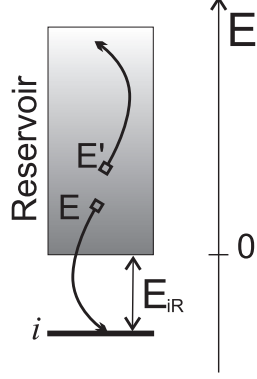


FIG. 1: Schematic representation of the exciton-exciton interaction in the reservoir leading to the scattering towards the quantized polariton states. The reservoir has a 2D (constant) density of states with a thermal distribution function.

vary above the width given by the pumping laser spot size. We used $W_{XX} = 2 \cdot 10^3 \text{ s}^{-1}$, $W_{XP} = 10^9 \text{ s}^{-1}$, $w_r = 3 \mu\text{m}$.

In order to understand the terms in the Boltzmann equation, let us consider for example the case of the scattering from the reservoir towards a quantized state i and backward assisted by exciton-phonon and exciton-exciton interaction. We neglect the final state stimulation within the reservoir which means that we assume a weak occupation ($n_R(E) \ll 1$) of these states. In all cases, the energy difference between the state i and the bottom of the exciton reservoir is E_0 .

Let us first consider the most complicated case of the forward scattering assisted by exciton-exciton interaction (sketched in figure S-1). In order to calculate the corresponding scattering rate, we have to sum over all possible scattering events. The corresponding scattering rates reads:

$$W_{XX} I_{iRRR} (n_i + 1) \sum_{E=0}^{\infty} n_R(E) \sum_{E'}^{\infty} n_R(E') (1 + n_R(E' + E + E_{iR})) \approx W_{XX} I_{iRRR} (n_i + 1) N_R^2 \quad (5)$$

The rate is proportional to N_R^2 and is similar to a scattering rate written between individual states and based on particle-particle interaction. The backward process of one particle going from the quantized states to the reservoir reads:

$$\begin{aligned}
& W_{XX} I_{iRRR} n_i \sum_{E=0}^{\infty} (1 + n_R(E)) \sum_{E'=0}^{\infty} n_R(E' + E + E_{iR}) (1 + n_R(E')) \\
& \approx W_{XX} I_{iRRR} n_i \sum_{E=0}^{\infty} (1 + n_R(E)) e^{-\frac{E+E_{iR}}{kT}} \sum_{E'=0}^{\infty} n_R(E') \\
& \approx W_{XX} I_{iRRR} n_i N_R e^{-\frac{E_{iR}}{kT}} \sum_{E=0}^{\infty} e^{-\frac{E}{kT}} = W_{XX} I_{iRRR} n_i \frac{N_R^2}{n_R(0)} e^{-\frac{E_{iR}}{kT}} = W_{XX} I_{iRRR} \frac{S m k T}{2 \pi \hbar^2} n_i N_R e^{-\frac{E_{iR}}{kT}}
\end{aligned} \tag{6}$$

The rate is similar to the one of the forward process except by the term : $e^{-\frac{E_{iR}}{k_B T}}/n_R(0)$. The relaxation of particles toward a low energy state is therefore favored only for a minimum energy difference $E_0 > k_B T \ln(n_R(0))$.

For the phonon-assisted scattering between the reservoir R and a quantized state i the expressions are quite similar. The scattering rates from the reservoir towards the state i reads:

$$W_{XP} I_{iR} (n_i + 1) \sum_E n_R(E) (1 + n_{ph}(E + E_{iR})) \approx W_{XP} I_{iR} (n_i + 1) N_R \tag{7}$$

The scattering rates from the state i toward the reservoir reads:

$$W_{XP} I_{iR} n_i \sum_{E=0}^{\infty} n_{ph}(E) (1 + n_R(E)) \approx W_{XP} I_{iR} n_i e^{-E_{iR}/k_B T} \frac{S k_B T}{2 \pi \hbar^2} \tag{8}$$

One can note that the expressions for the scattering processes involving exciton reservoir and phonons are quite similar. This is explained by the fact that excitonic reservoir is assumed to be thermalized at the lattice temperature.

Despite the complexity of the equations used in our simulation, we would like to underline that the number of fitting parameter is really limited.

Figure2 presents calculations corresponding to the experiments described in fig.4 of the paper. The reservoir is injected in the left pillar. The difference with the calculations presented in fig.4 is that here the scattering rates are taken constant, equal to that obtained at low excitation density. Thus we neglect the effect of the polariton wavefunction renormalization on the scattering rates. Clearly the main features of the experiments are not well described, in particular condensation in the metastable state at intermediate excitation powers is not reproduced.

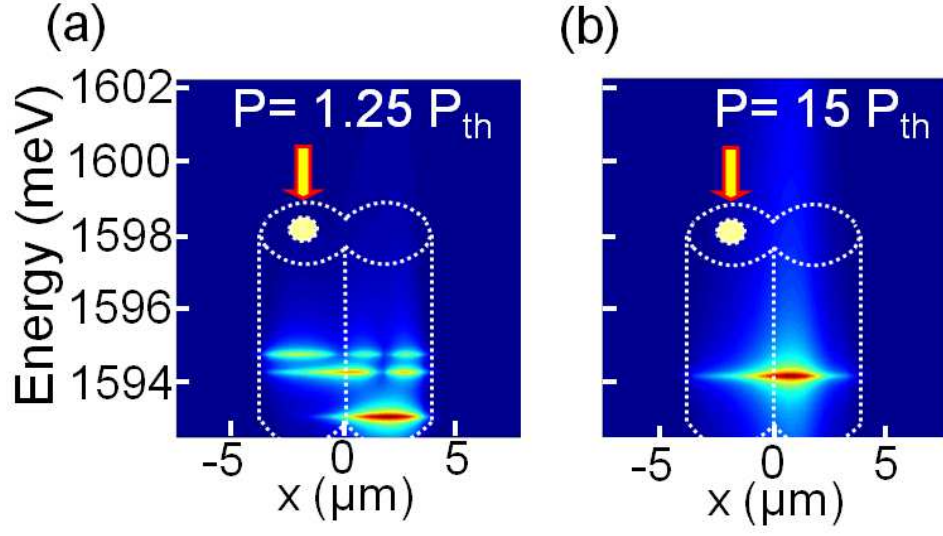


FIG. 2: Calculated emission pattern considering a reservoir potential proportional to the excitation power in the left micropillar but without taking into account the changes in the scattering rates.

The crucial ingredient which allows catching the basic physics in our experiments is to take into account the overlap integrals between initial and final states in the scattering rates. As shown in the paper, these wave functions are strongly distorted by interactions, and this dramatically modifies the way polariton relaxation occurs in the system.